Analytical Methods

PAPER

View Article Online
View Journal | View Issue

Cite this: *Anal. Methods*, 2025, **17**, 6160

Development of a natural product-based selective fluorescent sensor for Cu^{2+} and DNA/protein: insights from docking, DFT, cellular imaging and anticancer activity†

Sourav Pakrashy,‡[a] Manik Das,‡[a] Sounik Manna,[b] Sujata Maiti Choudhury,[b] Hazeena Shinziya,[c] Bhriguram Das,[d] Malay Dolai *[a] and Avijit Kumar Das *[c]

Received 7th May 2025
Accepted 3rd July 2025

DOI: 10.1039/d5ay00778j

rsc.li/methods

The natural product seselin (**SS**), was synthesized and characterized spectroscopically for the selective detection of Cu^{2+} and biomolecules such as ct-DNA and BSA. The probe exhibits strong bluish emission in a MeOH–H_2O (7 : 3, v/v) HEPES buffer solution (pH 7.4) at 453 nm. Upon exposure to Cu^{2+}, the **SS** solution shows a selective fluorescence 'turn-off' with a binding constant of 2.13×10^5 M^{-1} and a detection limit of 3.48×10^{-8} M. The HOMO–LUMO energy gap of the probe **SS** decreases from ΔE = 7.97 eV to ΔE = 7.77 eV upon binding with Cu^{2+}, indicating enhanced stability due to ligand–metal complex formation. Significantly, the ligand **SS** exhibits fluorescence enhancement in the presence of ct-DNA and BSA, resulting in a visible fluorescence change from colorless to blue, with binding constants of 4.8×10^4 M^{-1} and 4.7×10^4 M^{-1}, respectively. The binding interactions of **SS** with biomacromolecules have been explored through molecular docking studies, revealing that the probe can serve as a promising anti-cancer and anti-viral agent. Furthermore, the probe **SS** demonstrates potent anticancer activity in treatments involving MCF-7 and HLC cells. Additionally, the probe **SS** is capable of detecting intracellular Cu^{2+} in live MCF-7 cell lines.

1. Introduction

Polyphenols are secondary metabolites with wide distribution in the plant kingdom. Heterocyclic polyphenols hold significant importance in chemistry due to their diverse applications in drug development, photochemistry, agrochemicals, dyes, and more.[1] Notably, the pyranocoumarin framework stands out as a highly promising heterocyclic structure present in both natural and synthetic compounds. It exhibits a wide range of biological activities, including anti-inflammatory, anti-HIV, antitubercular, anti-HBV, anti-dyslipidemic, antiplatelet, anti-oxidant, and antibacterial properties.[2–4] Seselin, a pyranocoumarin, has been isolated from roots of shamouti orange, sour orange, sweet lime and grapefruit.[5] Seselin significantly influences root development by inhibiting radicle growth in cucumber, lettuce, radish, and wheat seedlings cultivated in darkness.[6] Seselin exhibits DNA-damaging properties and demonstrates cytotoxic effects against various cell lines, including Vero monkey cells, L1210 murine leukemia, CEM leukemia, SW1573 lung tumor, and P-388 lymphocytic leukemia.[7–9] Naturally occurring seselin-type coumarins, such as anomalin, have been shown to suppress skin tumor promotion and counteract the TNF-β-induced reduction in L929 cell viability.[10] However, the chemosensing applicability of seselin has not been disclosed exclusively. Among the different methods available for studying chemosensing behavior, the fluorimetric method is considered as versatile by researchers due to its several advantages like operational simplicity, low cost, super sensitivity, *etc.* However, only a small percentage of fluorescent probes are derived directly from natural sources; most are synthesized through organic reactions with certain hazardous chemicals and laborious procedures.[11] Furthermore, compared to synthetic dyes, natural dyes have superior biodegradability, are derived from renewable resources, and exhibit environmentally favourable properties.[12,13]

In this context, selective detection of analytes like Cu^{2+} cations by seselin is highly important as copper is an important cation involved in biological processes in both plants animals.

[a]*Department of Chemistry, Prabhat Kumar College, Purba Medinipur 721404, WB, India. E-mail: dolaimalay@yahoo.in*

[b]*Biochemistry, Molecular Endocrinology, and Reproductive Physiology Laboratory, Department of Human Physiology, Vidyasagar University, Midnapore 721102, WB, India*

[c]*Department of Chemistry, Christ University, Hosur Road, Bangalore, Karnataka, 560029, India. E-mail: avijitkumar.das@christuniversity.in*

[d]*Department of Chemistry, Vidyasagar University, Paschim Medinipur 721102, WB, India*

† Electronic supplementary information (ESI) available. See DOI: https://doi.org/10.1039/d5ay00778j

‡ These authors contributed equally.

It is a constituent of different enzymes, proteins, and vitamins required for mammals. An excess and deficiency of Cu^{2+} may cause various health issues.[14] Copper is the third most abundant soft transition metal in the human body, following iron and zinc. In a healthy adult, the total copper content is approximately 80 mg, with the highest levels present in the liver and brain. As an essential trace element for higher plants and animals, copper plays a vital role in numerous physiological processes, including iron and zinc metabolism, free radical elimination, bone development, and the production of skin and hair pigments. An imbalance in copper levels, whether deficiency or excess, can lead to diseases such as Menkes disease, Wilson's disease, and cancer.[15] Therefore, accurate monitoring and detection of Cu^{2+} levels are crucial. Although many chemosensors and chemodosimeters for Cu(II) have been developed, limitations remain, including complex synthesis, high detection limits, dependence on organic solvents, and interference from coexisting transition metals with similar reactivity.[16–18] Although different synthetic materials and methods have been designed and reported for Cu^{2+} sensing, the reports on the use of natural product-based phytochemicals for the selective detection of copper ion are relatively rare (Table S1, ESI†).

Furthermore, molecular docking is a powerful computational technique that serves a key tool in drug discovery and structural molecular biology.[19,20] Molecular docking is a computational technique used to model the interaction between small molecules and proteins at the atomic level. This approach helps in understanding the behavior of small molecules within the binding site of target proteins and provides insights into fundamental biochemical processes.[21,22] Docking can save time and money in the drug development process, determine the structure of proteins with unknown structures, study protein interactions, support drug discovery, predict side effects and biodegradation, and help understand how enzymes work and how they interact with ligands.[23–27] **SS** can disrupt the activity of Src, GSK-3β, and ERK cancer cells, cooperate with cisplatin to promote the phosphorylation of p53 in cells, and then stimulate the activity of caspase-3 in cells and cause cell death.[28] In this work, we performed docking studies of **SS** with DNA and protein. Seselin alleviated sepsis induced by caecal ligation and puncture, reducing pro-inflammatory factor levels and inhibiting STAT1 and p6 activity. Its anti-inflammatory effects are attributed to modulation of Jak2 activity.[29] Therefore, we have utilized the phytochemical **SS** for the detection of copper and DNA/protein in solution as well as in live cells along with docking studies to further explore its potential. The phytochemical **SS** has been characterized by ^{1}H NMR and mass spectrometry (Fig. S1–S3†).

2. Experimental section

2.1 Material and methods

The materials and the methods of the study are described in the ESI.† The detailed photophysical studies (solution preparation, fluorescence study, binding constant determination,[30,31] detection limit,[32] *etc.*), DFT calculations,[33–41] molecular docking[19,21,42–44] and bio-imaging[32,45,46] are described in the ESI.†

2.2 Synthesis of seselin (SS)

The total synthesis of seselin was carried out in two steps as shown in Scheme 1.

2.2.1 Synthesis of umbelliferone (3). 4-Hydroxy salicylaldehyde (**1**) [0.5 mmol], ethyl 3-(trimethylsilyl) propiolate (**2**) [0.5 mmol] and CuI [0.05 mmol] were taken in a clean and dry 10 ml round-bottom flask. Then, dichloromethane [3 ml] was added to it under stirring, followed by the addition of Et_3N [1.0 mmol]. The reaction mixture was stirred overnight. After completion of the reaction (confirmed by TLC monitoring), it was quenched with 1(N) HCl and then worked up; the combined organic layer was washed with brine solution and eventually extracted with DCM. Umbelliferone was purified by column chromatography with ethyl acetate in petroleum ether (1 : 7) as the eluent (yield: 94%). ^{1}H NMR (DMSO-d_6, 400 MHz): δ (ppm): 6.13 (1H, d), 6.68 (1H, d), 6.76 (1H, s), 7.47 (1H, d), 7.87 (1H, d), 10.47 (1H).

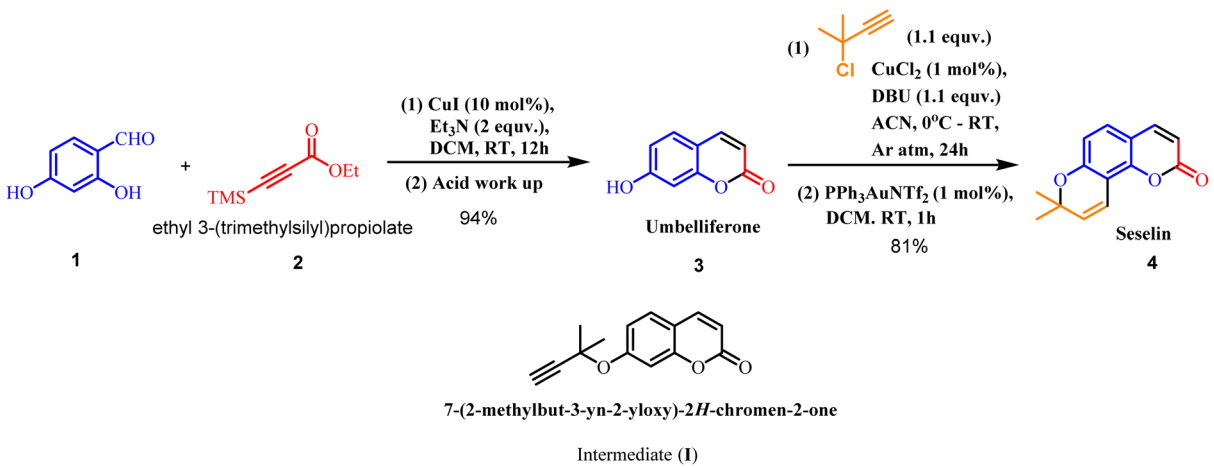

Scheme 1 Total synthesis of seselin.

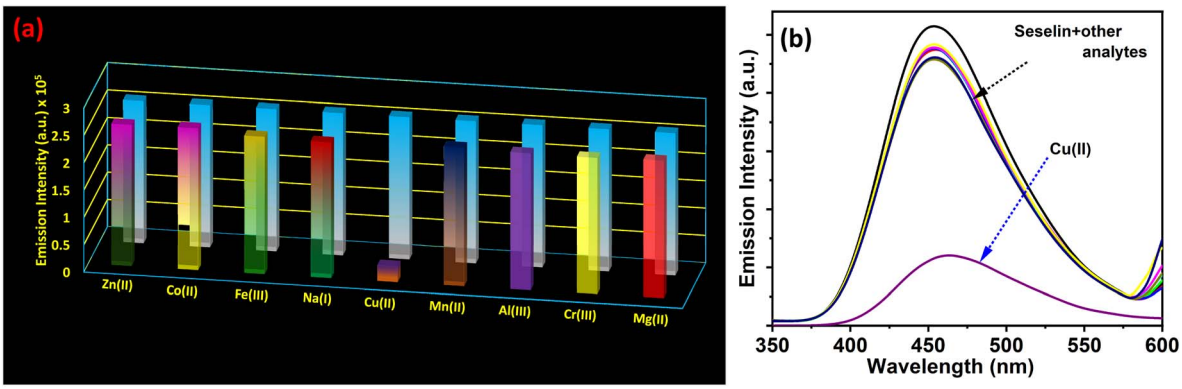

Fig. 1 (a) Change in emission intensity of **SS** (5×10^{-6} M) in the presence of various interfering metal ions (2×10^{-5} M). (b) Corresponding fluorescence spectra in MeOH–H_2O (7 : 3, v/v) HEPES buffer medium at pH 7.4 upon excitation at 330 nm. In the UV-vis spectroscopic analysis of **SS** (5×10^{-6} M) with Cu^{2+} (2×10^{-5} M) in a MeOH–H_2O (7 : 3, v/v) HEPES buffer solution at pH 7.4, a pronounced ligand absorption peak at 330 nm gradually decreased upon incremental addition of Cu^{2+} ions. Concurrently, a red-shifted absorption band emerged at 400 nm, accompanied by a distinct isosbestic point at 370 nm (Fig. S7†). These significant spectral changes, particularly the red-shifted band, suggest strong interaction between **SS** and Cu^{2+} ions.

2.2.2 Synthesis of seselin (4). Umbelliferone (**3**) [0.3 mmol] and 3-chloro-3-methylbut-1-yne [0.33 mmol] were taken in a clean and oven-dried 10 ml reaction vial along with $CuCl_2$ [0.003 mmol] as the catalyst and DBU [0.33 mmol] as the base in acetonitrile solvent at ice-bath temperature. The reaction was then allowed to proceed at ambient temperature under an argon atmosphere for 24 h to get the substitution product intermediate I. Then, intermediate I without purification was treated with $Ph_3PAuNTf_2$ [0.003 mmol] as the catalyst for eventual annulation in dichloromethane at room temperature for an hour in the same reaction pot (after evaporation of the acetonitrile solvent) to obtain the target product seselin (**4**) after work up with dichloromethane. Seselin was purified by column chromatography with ethyl acetate in petroleum ether (1 : 10) as the eluent (yield: 81%). The melting point was determined in open capillary tubes using a Köfler block apparatus and was found to be 119.6 °C.

^{1}H NMR ($CDCl_3$, 400 MHz): δ (ppm): 1.49 (6H, s), 5.7 (1H, d), 6.2 (1H, d), 6.7 (1H, d), 6.9 (1H, d), 7.2 (1H, d), 7.63 (1H, d). ESI-MS: 229.0 (found), 228.07 (calcd.). ^{13}C NMR ($CDCl_3$, 100 MHz): δ (ppm): 161.11, 156.33, 150.12, 143.96, 130.79, 127.79, 115.02, 113.56, 112.63, 109.32, 28.14.

3. Results and discussion

3.1 Spectroscopic response of SS towards several cations

Spectroscopically to check the sensing behavior of the probe **SS** towards various cations, fluorescence spectra of **SS** (5×10^{-6} M) was recorded in the presence of different metal ions in MeOH–HEPES buffer (7 : 3 v/v). The probe exhibits strong fluorescence at 453 nm ($\phi = 0.197$) upon excitation at $\lambda_{ex} = 330$ nm (Fig. 1). Before continuing the sensing process, the pH stability of the probe as well as its stability in the working buffer solution were investigated for its biomedical application. In this context, the emission change of **SS** was separately recorded by varying the pH of the solvent (pH = 2–12). The results show that it is highly emissive in neutral-pH or even in slightly high-pH solutions, exhibiting the highest emission capabilities (Fig. S4†). The fluorescence spectra were recorded over time and it was observed that there was minimal change in the fluorescence

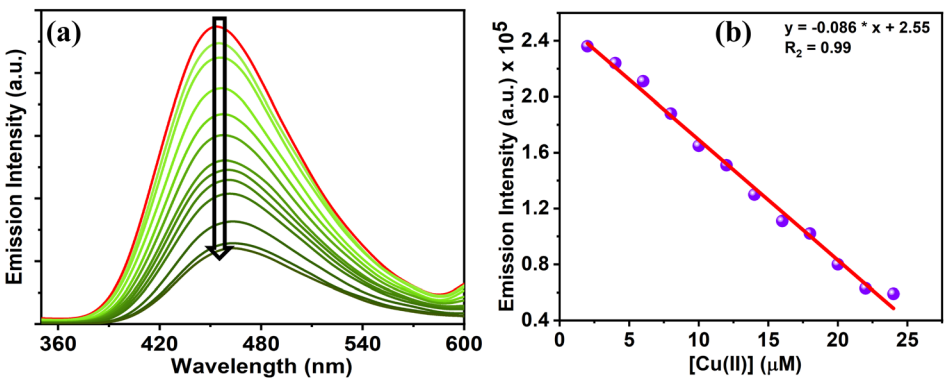

Fig. 2 (a) Change in emission intensity of **SS** (5×10^{-6} M) after incremental addition of Cu(II)(1–25 μM) in MeOH–H_2O (7 : 3 v/v) HEPES buffer solution at pH 7.4. (b) Determination of the LOD value of **SS** for Cu(II) ions.

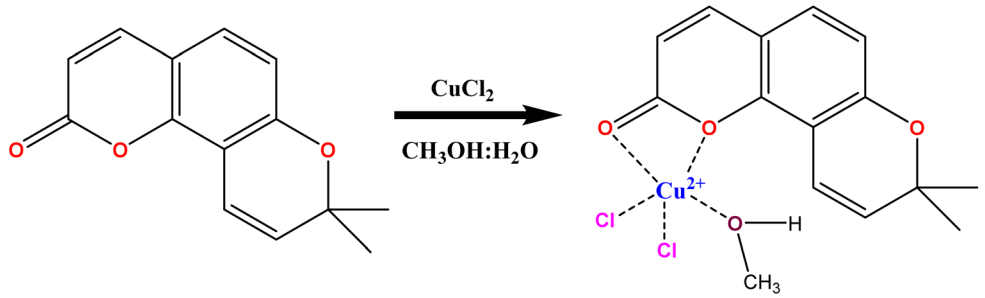

Scheme 2 Probable binding mode of **SS** with Cu^{2+} complex in methanol–water medium.

spectra of the probe, indicating that it was stable in the working buffer medium (Fig. S5†). After standardizing the pH of the buffer, the fluorescence spectra were recorded in MeOH–HEPES buffer medium (7 : 3 v/v) at pH 7.4. Herein, it was observed that among several cations, only in the presence of Cu(II) ions, the fluorescence intensity of the probe was quenched while other cations did not make any significant change in the fluorescence response of the probe (Fig. 1). This result suggests that the natural product **SS** can act as a selective sensor for Cu^{2+}.

3.1.1 Fluorescence titration of SS with Cu(II). To demonstrate the sensitivity of **SS** towards Cu(II), a fluorescence study was performed at a fixed concentration of the probe **SS** (5×10^{-6} M) in MeOH–HEPES buffer solution (7 : 3, v/v). Initially **SS** exhibited strong fluorescence due to its conjugated π-electron system, which spans the fused coumarin and furan rings. Moreover, the rigid planar structure of seselin reduces non-radiative decay pathways, enhancing emission intensity at 453 nm. Additionally, the presence of electron-donating and withdrawing groups on the coumarin moiety can influence its photophysical behavior by modulating the energy gap between the excited and ground states. From the titration profiles, it was observed that upon incremental addition of Cu(II) (1–25 μM) to the ligand solution, the fluorescence intensity at 453 nm was gradually diminished with a red shift in the emission maxima ($\Delta\lambda = 10$ nm) (Fig. 2a). The Cu^{2+} ion has an open shell d^9 electronic configuration and exhibits notable quenching response on binding with **SS** due to the chelation enhanced quenching (CHEQ) effect.[47,48] The formation of the **SS**–Cu^{2+} complex was confirmed by the appearance of a mass peak at $m/z = 393$ (calculated mass: 392.97) (Fig. S9†), corresponding to the [Cu(**SS**)$(Cl)_2$(MeOH)] ensemble (Scheme 2). From the titration plot of emission intensity *vs.* metal concentration, the detection limit (LOD) of **SS** towards Cu(II) was calculated to be 3.48×10^{-8} M (Fig. 2b). From linear fitting and the intercept of the titration plot, the binding constant was calculated to be 2.13×10^5 M^{-1} (Fig. S10†) and through Job's plot analysis, the 1 : 1 binding stoichiometry for **SS**–Cu^{2+} complexation was verified (Fig. S8†).

3.2 Reversibility and interference performance

Reversibility and reproducibility are crucial attributes for sensors, offering significant advantages for sustainable research and practical applications. During the sensing of Cu(II), the reversibility of **SS** can be achieved by the alternative addition of Cu(II) ions and ethylenediaminetetraacetic acid (EDTA) into the **SS**–Cu(II) complex solution. Here EDTA acts as a masking agent for Cu(II). From experimental results, it has been observed that this reversible cycle can be performed up to 10 times with a marked contrast in emission intensity alternation (Fig. 3a).

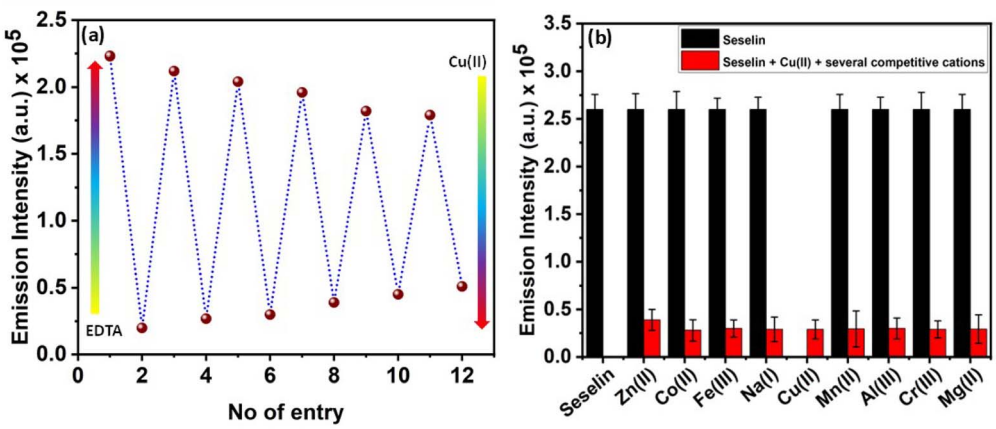

Fig. 3 (a) Reversibility experiment of **SS** by alternate addition of Cu(II) and EDTA in MeOH–H_2O (7 : 3 v/v) HEPES buffer solution. (b) Change in emission intensity of the **SS**–Cu(II) conjugate in the presence of several competitive cations in MeOH–H_2O (7 : 3 v/v) HEPES buffer solution.

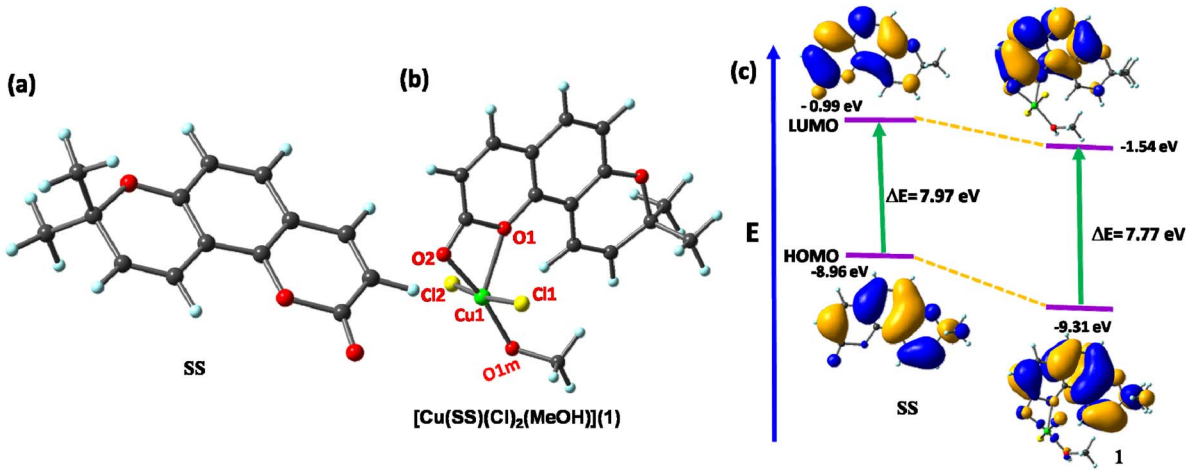

Fig. 4 Geometry-optimized molecular structure of (a) SS (L) and (b) $[Cu(L)(Cl)_2(MeOH)]^{2+}$(1); (c) Frontier molecular orbitals of SS and 1.

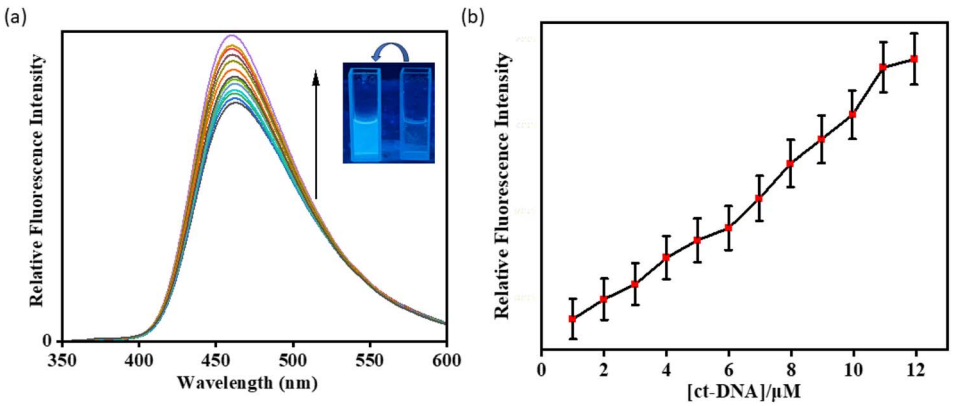

Fig. 5 (a) Fluorescence titration of SS ($c = 2.0 \times 10^{-5}$ M) upon incremental addition of ct-DNA ($c = 2$ mM) in Tris–HCl buffer, pH = 7.2. (b) Concentration *vs.* intensity changes of SS with ct-DNA.

To explain the interference by other competitive cations during the sensing of Cu(II), emission spectra of the **SS**–Cu(II) complex in the presence of several competitive cations were recorded and no significant interference from any other metal ions was observed in the binding of **SS** with Cu(II) (Fig. 3b).

3.3 Geometry optimization and electronic structure

The optimized geometries of the probe **SS** and its Cu(II) complex are depicted in Fig. 4a. HRMS data confirmed the composition of the complex as [Cu(**SS**)$(Cl)_2$(MeOH)](**1**), which was subsequently subjected to theoretical geometry optimization using

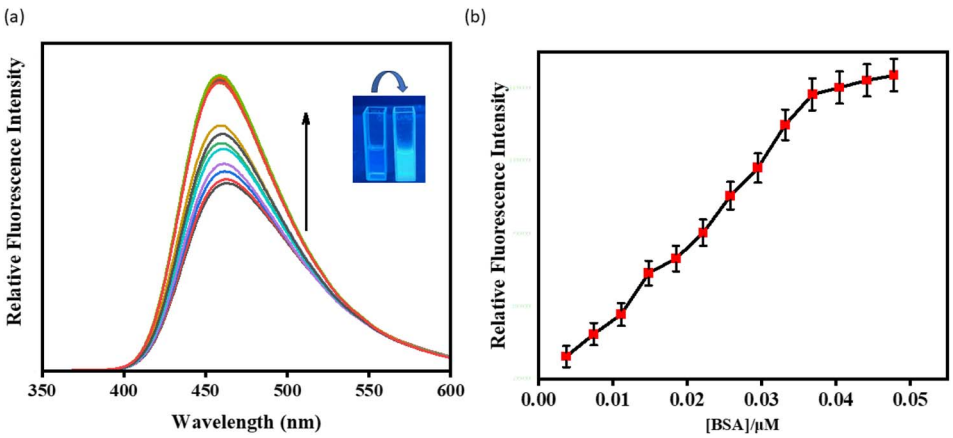

Fig. 6 (a) Fluorescence titration of SS ($c = 2.0 \times 10^{-5}$ M) upon incremental addition of BSA protein ($c = 2$ mM) in Tris–HCl buffer, pH = 7.2. (b) Concentration *vs.* intensity changes of SS with BSA protein.

Table 1 Results of **SS** docking with proteins

Name of targeted proteins	PDB ID	**SS** docking score (kcal mol^{-1})
BSA in complex with ketoprofen	6QS9	−8.7
BSA in complex with naproxen	4OR0	−9.4

Table 2 Results of **SS** docking with DNA

Name of targeted DNAs	PDB ID	**SS** docking score (kcal mol^{-1})
Structure of a B-DNA dodecamer	1BNA	−7.4

the DFT/B3LYP method. The positive and negative phases are illustrated in orange and blue, respectively.

The metal center Cu^{2+} is penta-coordinated in complex **1** with a neutral bi-dentate ligand (L) (with O_2 donor sites), two Cl^- ions and one MeOH molecule as solvent, adopting a distorted square pyramidal geometry to form $[Cu(\mathbf{SS})(Cl)_2(MeOH)]$ (**1**). The calculated Cu–O and Cu–Cl bond distances fall in the range of 1.94–2.11 Å and 2.11–2.12 Å respectively. Interestingly, it was observed that upon formation of the monomeric complex with probe **SS**, the HOMO–LUMO energy gap ($\Delta E = 7.77$ eV for **1**) decreases compared to that of the bare probe ($\Delta E = 7.97$ eV) (Fig. 4b).

3.4 Fluorometric binding study of SS with DNA and protein BSA

The fluorescence experiments of **SS** with DNA/protein have been performed in Tris–HCl buffer at pH = 7.2. In the emission spectra, **SS** showed a weak emission signal at 462 nm ($\lambda_{ex} = 330$ nm) in the absence of ct-DNA and BSA. However, the increasing concentration of ct-DNA and BSA in the **SS** solution led to significant fluorescence enhancement at 460 nm and 458 nm, respectively (Fig. 5 and 6). The detection limits of **SS** for ct-DNA and BSA from fluorescence measurements are 1.05 μM and 0.0024 μM, respectively (Fig. S11†). The binding constants of **SS** with ct-DNA and BSA obtained from non-linear fitting curves of spectrofluorometric titrations are 4.8×10^4 M^{-1} and 4.7×10^4 M^{-1}, respectively (Fig. S12†). The enhancement of the

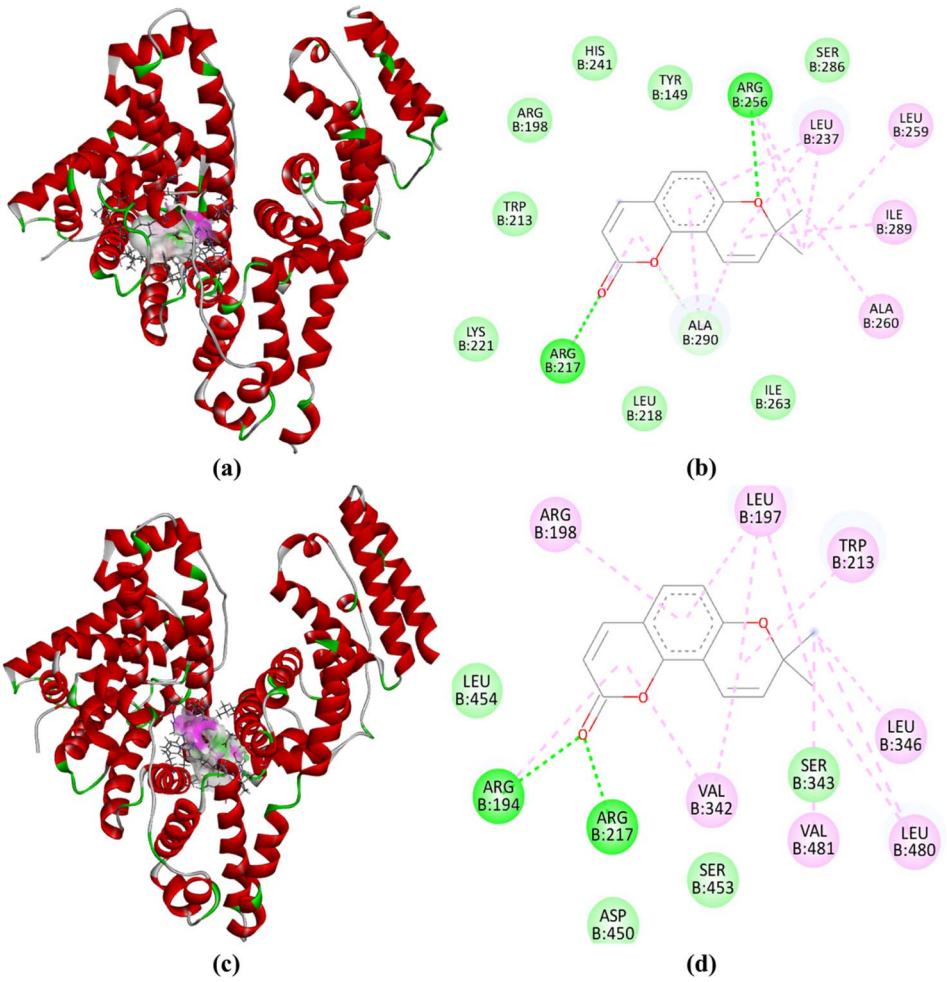

Fig. 7 (a) Pictorial observation of the docked **SS** inside the active site of 6QS9, with an engrossed (b) 2D interpretation of its interaction with binding site amino acid residues. (c) Pictorial observation of the docked **SS** inside the active site of 4OR0, with an engrossed (d) 2D interpretation of its interaction with binding site amino acid residues.

fluorescence response of **SS** on binding with ct-DNA and BSA is due to the polarity of the binding cavities, where the CS or ICT state of **SS** is stabilized more efficiently inside the more polar DNA and protein binding cavity.[49] The detailed interaction pathways of **SS** with DNA and proteins have been explained through molecular docking analysis.

3.5 Docking study of SS with biomacromolecules

The BSA proteins PDB-ID: 6QS9 (bovine serum albumin in complex with ketoprofen) and 4OR0 (crystal structure of bovine serum albumin in complex with naproxen) showed strong binding with **SS**. The calculations reveal the maximum free energy change for these interactions as $\Delta G = -8.7$, and -9.4 kcal mol^{-1} (Table 1).

The binding energy between **SS** and CT-DNA (PDB-ID: 1BNA), from docking calculations, reveals a maximum free energy change of $\Delta G = -7.4$ kcal mol^{-1} (Table 2).

Fig. 7a presents the docked **SS** at the active site of 6SQ9 with two hydrogen bonds between the ligand and the 217th and 256th ARG residues of chain B (Fig. 7b), and Fig. 7c presents the docked **SS** at the active site of 4OR0 with two hydrogen bonds between the ligand and the 194th and 217th ARG residues of chain B (Fig. 7d).

Fig. 8 reveals the binding of docked **SS** with the B-DNA dodecamer (1BNA), showing a hydrogen bond interaction with the 16th DG residue of chain B. Thus, the docking results with these bio-macromolecules predict that it has good binding properties and can be considered a potent inhibitor for the development of new cancer treatment drugs.

3.6 Anticancer activity of SS and biosensor imaging

The docking study shows that the probe has good anti-cancer activity. To verify this prediction, cytotoxicity was evaluated experimentally using MCF 7 and HLCs cell lines according to the standard protocol. Moreover, an *in vitro* cell imaging study with **SS** was also performed to explore the biological utility of the probe for Cu^{2+}.

3.6.1 Cell viability study on MCF 7 and human lymphocyte cells (HLCs). The cytotoxicity of **SS** against MCF-7 cells was assessed using the MTT assay. The results demonstrated that **SS** significantly reduced cell viability in a dose-dependent manner showing strong cytotoxic activity against these cells. The IC_{50} value of **SS** was found to be 23.17 μg ml^{-1}, which is comparable to the IC_{50} value of the standard anticancer drug 5-FU (16.14 μg ml^{-1}), demonstrating that **SS** also has a cytotoxic effect (Fig. 9a). A time-dependent cell viability study exhibited that **SS** inhibited cell viability by 53.87% and 40.16%, at 24 h and 48 h, respectively (Fig. 9b). These findings clearly demonstrate the cytotoxic potential of **SS** against MCF-7 cells. Furthermore, **SS** did not exhibit significant toxicity to lymphocytes at doses up to 50 μg ml^{-1}, with only a slight reduction in lymphocyte viability observed (Fig. 9c). These findings suggest that **SS** could be a potent anticancer agent for use in treatments involving MCF-7 cells.

3.6.2 Bio-imaging study. During one-hour incubation at 37 °C with **SS** at its IC_{50} concentration, intense intracellular blue fluorescence was detected, indicating high intensity of **SS** inside the cells. However, when cells were incubated with an external Cu^{2+} ion solution, no notable intracellular emission was observed. **SS** easily penetrated the cell membrane and showed

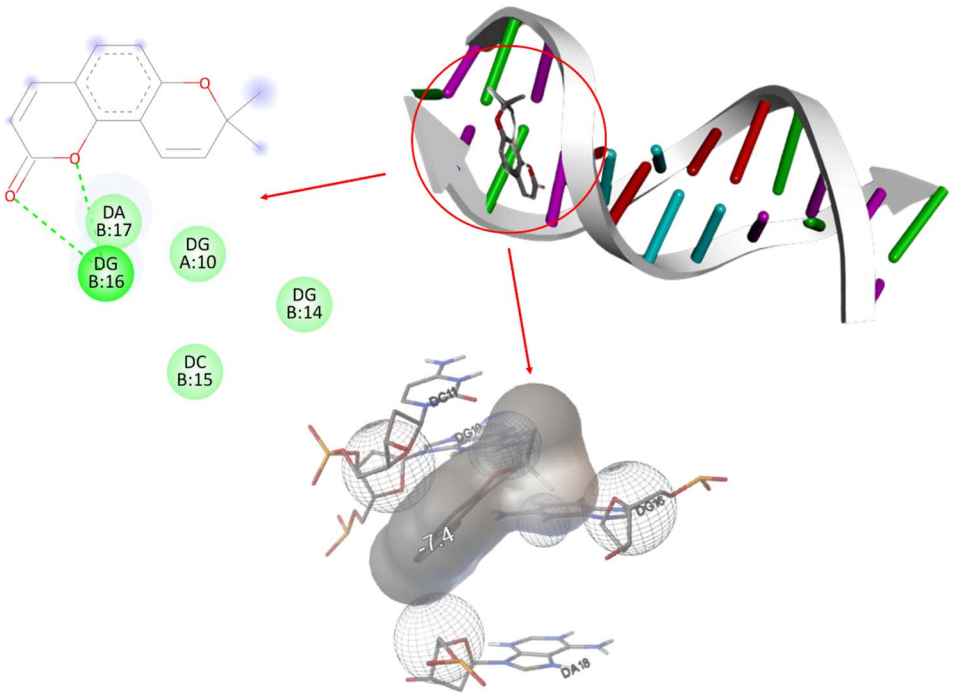

Fig. 8 Pictorial representation of the docked SS inside the active site of the DNA-binding protein 1BNA, providing a detailed understanding of its interaction with nucleotides.

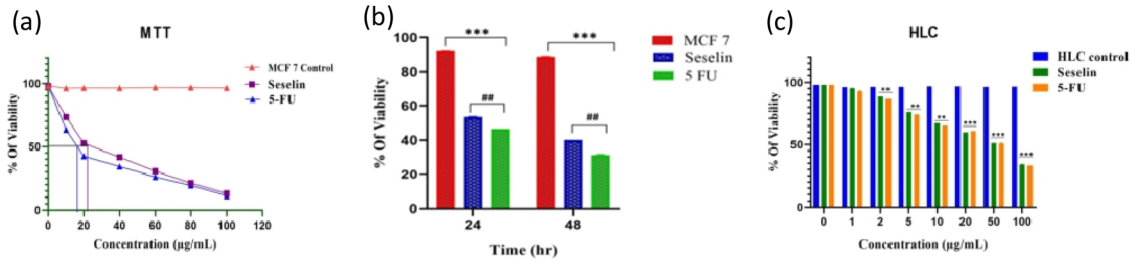

Fig. 9 (a) The cytotoxic effect of SS on MCF-7 cells was evaluated at different concentrations. (b) Cell viability was assessed at 24- and 48-hours following treatment with SS, and the IC_{50} value was determined. The results are presented as mean ± SEM ($n = 3$); ***$p < 0.001$, #$p < 0.05$, ##$p < 0.01$, and ###$p < 0.001$; * compared with the control; # compared with 5-FU. (c) A minimal reduction in lymphocyte viability was observed at SS concentrations as high as 50 µg ml^{-1}. Data are expressed as mean ± SEM from three independent experiments; **$p < 0.01$ and ***$p < 0.001$ compared to the control group.

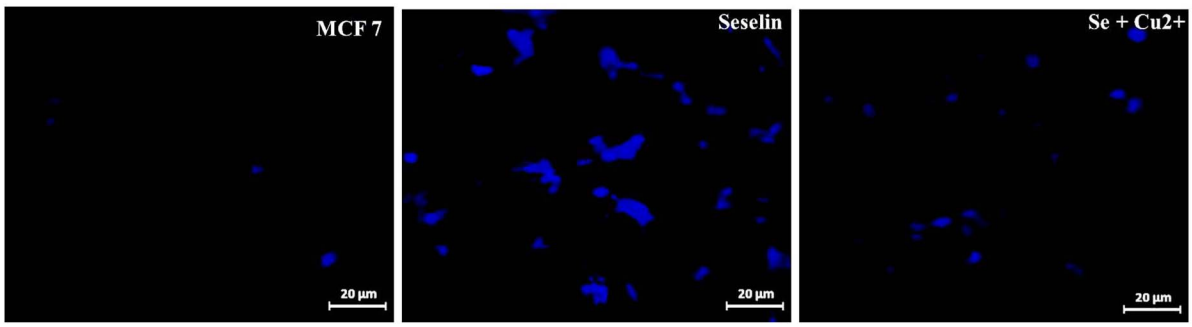

Fig. 10 Intercellular biosensor cell imaging study performed on MCF7 cells. Cells were incubated with free SS and brighter blue fluorescence was observed compared to the SS + Cu^{2+} treated groups.

blue fluorescence but when **SS** was incubated with Cu^{2+} ions, the fluorescence images did not show significant blue fluorescence for the formation of the **SS**–Cu^{2+} complex (Fig. 10). These findings suggest that **SS** could act as a selective sensor for detecting Cu^{2+} ions in bio-imaging at specific concentrations and incubation times.

4. Conclusion

The natural product seselin (**SS**) was synthesized and characterized spectroscopically, exhibiting strong bluish emission at 453 nm. In the presence of Cu^{2+}, the probe solution showed a turn-off sensing phenomenon among various cations, with the binding constant and detection limit determined to be 2.13 × 10^5 M^{-1} and 6.97 × 10^{-8} M, respectively. DFT calculations revealed that the binding of Cu^{2+} with **SS** decreases the HOMO–LUMO energy gap from $\Delta E = 7.97$ eV to $\Delta E = 7.77$ eV, indicating stable complex formation between the ligand and metal. Notably, the ligand **SS** displays fluorescence enhancement in the presence of ct-DNA and BSA, resulting in a visible fluorescence change from colorless to blue. The binding constants were determined to be 4.8 × 10^4 M^{-1} and 4.7 × 10^4 M^{-1}, respectively. The probe **SS** also exhibits promising anticancer and antiviral properties, as supported by docking studies with DNA biomacromolecules. Furthermore, the potent anticancer activity of **SS** was confirmed by an MTT assay using MCF-7 and HLC cells. Moreover, the probe **SS** is capable of detecting intracellular Cu^{2+} in live MCF-7 cells.

Data availability

The data supporting this article have been included as part of the ESI.†

Conflicts of interest

There are no conflicts of interest to declare.

Acknowledgements

MD acknowledges the Science & Engineering Research Board (SERB), Govt. of India (ref no. PDF/2016/000334). Avijit Kumar Das specially acknowledges the State University Research Excellence (SERB-SURE) programme of the Science and Engineering Research Board (SERB) (File Number: SUR/2022/002461) under the Anusandhan National Research Foundation (ANRF) and the Department of Science and Technology (DST), Government of India, for the financial support through the research grant.

References

1 J. Jampilek, *Molecules*, 2019, **24**, 3839.

2 C.-R. Su, S. F. Yeh, C. M. Liu, A. G. Damu, T.-H. Kuo, P.-C. Chiang, K. F. Bastow, K.-H. Lee and T.-S. Wu, *Bioorg. Med. Chem.*, 2009, **17**, 6137–6143.
3 F. Salehian, H. Nadri, L. Jalili-Baleh, L. Youseftabar-Miri, S. N. Abbas Bukhari, A. Foroumadi, T. Tüylü Küçükkilinç, M. Sharifzadeh and M. Khoobi, *Eur. J. Med. Chem.*, 2021, **212**, 113034.
4 S. J. Min, H. Lee, M.-S. Shin and J. W. Lee, *Int. J. Mol. Sci.*, 2023, **24**, 10026.
5 E. Tomer, R. Goren and S. P. Monselise, *Phytochemistry*, 1969, **8**, 1315–1316.
6 R. Goren and E. Tomer, *Plant Physiol.*, 1971, **47**, 312–316.
7 K. Ostrowska, W. Olejarz, M. Wrzosek, A. Głuszko, G. Nowicka, M. Szczepański, I. B. Materek, A. E. Kozioł and M. Struga, *Biomed. Pharmacother.*, 2017, **95**, 1412–1424.
8 F. Nagase, K. Ueda, I. Nakashima, K. Kawashima, K. Isobe, E. Nagura, K. Yamada, T. Yokochi, Y. Hasegawa and T. Yoshida, *Int. J. Cancer*, 1986, **38**, 907–914.
9 J. F. Alhmoud, A. G. Mustafa and M. I. Malki, *Int. J. Mol. Sci.*, 2020, **21**, 7365.
10 H. Nishino, T. Okuyama, M. Takata, S. Shibata, H. Tokuda, J. Takayasu, T. Hasegawa, A. Nishino, H. Ueyama and A. Iwashima, *Carcinogenesis*, 1990, **11**, 1557–1561.
11 M. Rajasekar, V. Ranjitha and K. Rajasekar, *Results Chem.*, 2023, **5**, 100850.
12 D.-B. Sung and J. S. Lee, *RSC Med. Chem.*, 2023, **14**, 412–432.
13 S. Yadav, K. S. Tiwari, C. Gupta, M. K. Tiwari, A. Khan and S. P. Sonkar, *Results Chem.*, 2023, **5**, 100733.
14 R. A. Løvstad, *BioMetals*, 2004, **17**, 111–113.
15 (*a*) T. Chopra, S. Sasan, L. Devi, R. Parkesh and K. K. Kapoor, *Coord. Chem. Rev.*, 2022, **470**, 214704; (*b*) M. S. Kumar, S. Vishnu, M. Dolai, A. Nag, Y. Bylappa and A. K. Das, *Anal. Methods*, 2024, **16**, 676–685.
16 (*a*) M. Kumar, N. Kumar, V. Bhalla, P. R. Sharma and T. Kaur, *Org. Lett.*, 2012, **14**, 406–409; (*b*) S. Goswami, S. Maity, A. C. Maity, A. K. Maity, A. K. Das and P. Saha, *RSC Adv.*, 2014, **4**, 6300–6305; (*c*) S. Goswami, D. Sen, A. K. Das, N. K. Das, K. Aich, H. K. Fun, C. K. Quah, A. K. Maity and P. Saha, *Sens. Actuators, B*, 2013, **183**, 518–525; (*d*) S. Goswami, S. Maity, A. K. Das and A. C. Maity, *Tetrahedron Lett.*, 2013, **54**, 6631–6634.
17 (*a*) D. Wu, A. C. Sedgwick, T. Gunnlaugsson, E. U. Akkaya, J. Yoon and T. D. James, *Chem. Soc. Rev.*, 2017, **46**, 7105–7123; (*b*) S. Vishnu, A. Nag and A. K. Das, *Anal. Methods*, 2024, **16**, 5263–5271.
18 (*a*) S. Liu, Y. M. Wang and J. Han, *J. Photochem. Photobiol. C: Photochem. Rev.*, 2017, **32**, 78–103; (*b*) S. Vishnu, A. K. Das, Y. Bylappa, A. Nag and M. Dolai, *Anal. Methods*, 2024, **16**, 8164–8178.
19 P. C. Agu, C. A. Afiukwa, O. U. Orji, E. M. Ezeh, I. H. Ofoke, C. O. Ogbu, E. I. Ugwuja and P. M. Aja, *Sci. Rep.*, 2023, **13**, 13398.
20 X.-Y. Meng, H.-X. Zhang, M. Mezei and M. Cui, *Curr. Comput.-Aided Drug Des.*, 2011, **7**, 146–157.
21 A. Kukol, *Molecular Modeling of Proteins*, 2008.
22 A. E. Cho, V. Guallar, B. J. Berne and R. Friesner, *J. Comput. Chem.*, 2005, **26**, 915–931.
23 C. Guerrero-Perilla, F. A. Bernal and E. D. Coy-Barrera, *Rev. Colomb. Cienc. Quim.-Farm.*, 2015, **44**, 162–178.
24 G. Sliwoski, S. Kothiwale, J. Meiler and E. W. Lowe, *Pharmacol. Rev.*, 2014, **66**, 334–395.
25 L. Pinzi and G. Rastelli, *Int. J. Mol. Sci.*, 2019, **20**, 4331.
26 L. G. Ferreira, R. N. Dos Santos, G. Oliva and A. D. Andricopulo, *Molecules*, 2015, **20**, 13384–13421.
27 D. B. Kitchen, H. Decornez, J. R. Furr and J. Bajorath, *Nat. Rev. Drug Discovery*, 2004, **3**, 935–949.
28 R. Y. Shyu, C. H. Wang, C. C. Wu, L. K. Wang and F. M. Tsai, *Arch. Biol. Sci.*, 2023, **75**, 287–297.
29 L. Feng, Y. Sun, P. Song, L. Xu, X. Wu, X. Wu, Y. Shen, Y. Sun, L. Kong, X. Wu and Q. Xu, *Br. J. Pharmacol.*, 2019, **176**, 317–333.
30 H. A. Benesi and J. H. Hildebrand, *J. Am. Chem. Soc.*, 1949, **71**, 2703–2707.
31 R. Banerjee, R. Sinha and P. Purkayastha, *ACS Omega*, 2019, **4**, 16153–16158.
32 G. C. Das, B. Das, U. Saha, S. Kanta Dey, S. Maiti Choudhury, P. Brandao, A. A. Alothman, S. M. Wabaidur and M. Dolai, *Inorg. Chim. Acta*, 2024, 122404.
33 R. G. Parr, Density functional theory of atoms and molecules, in *Horizons of Quantum Chemistry: Proceedings of the Third International Congress of Quantum Chemistry Held at Kyoto, Japan, October 29 - November 3, 1979*, ed. K. Fukui and B. Pullman, Springer Netherlands, Dordrecht, 1980, pp. 5–15.
34 M. Cossi and V. Barone, *J. Chem. Phys.*, 2001, **115**, 4708–4717.
35 M. Cossi, N. Rega, G. Scalmani and V. Barone, *J. Comput. Chem.*, 2003, **24**, 669–681.
36 V. Barone and M. Cossi, *J. Phys. Chem. A*, 1998, **102**, 1995–2001.
37 A. D. Becke, *J. Chem. Phys.*, 1993, **98**, 5648–5652.
38 C. Lee, W. Yang and R. G. Parr, *Phys. Rev. B: Condens. Matter Mater. Phys.*, 1988, **37**, 785–789.
39 M. E. Casida, C. Jamorski, K. C. Casida and D. R. Salahub, *J. Chem. Phys.*, 1998, **108**, 4439–4449.
40 M. J. Frisch G. W. Trucks, H. B. Schlegel, G. E. Scuseria, M. A. Robb, J. R. Cheeseman, G. Scalmani, V. Barone, B. Mennucci, G. A. Petersson, H. Nakatsuji, M. Caricato, X. Li, H. P. Hratchian, A. F. Izmaylov, J. Bloino, G. Zheng and J. L. Sonnenberg, *Wall*, Gaussian Inc., Wallingford CT, 2009, DOI: **10.1007/s11172-018-2377-z**.
41 N. M. O'boyle, A. L. Tenderholt and K. M. Langner, *J. Comput. Chem.*, 2008, **29**, 839–845.
42 G. M. Morris and M. Lim-Wilby, *Methods Mol. Biol.*, 2008, **443**, 365–382.
43 S. Pakrashy, P. K. Mandal, S. K. Dey, S. M. Choudhury, F. A. Alasmary, A. S. Almalki, M. A. Islam and M. Dolai, *ACS Omega*, 2022, **7**, 33408–33422.
44 B. Das, S. Pakrashy, G. C. Das, U. Das, F. A. Alasmary, S. M. Wabaidur, M. A. Islam and M. Dolai, *J. Fluoresc.*, 2022, **32**, 1263–1277.
45 F. C. Hay and L. Hudson, *Practical Immunology*, Blackwell Scientific, 1989.

46 B. Das, K. C. Murmu, S. K. Dey, S. M. Chaudhuri, Z. M. Almarhoon, M. Z. Ansari, P. P. Bag and M. Dolai, *Inorg. Chem. Commun.*, 2024, **170**, 113108.
47 W. Yang, X. Chen, H. Su, W. Fang and Y. Zhang, *Chem. Commun.*, 2015, **51**, 9616–9619.
48 D. Udhayakumari, S. Naha and S. Velmathi, *Anal. Methods*, 2017, **9**, 552–578.
49 (*a*) A. Cuervo, P. D. Dans, J. L. Carrascosa and L. Fumagalli, *Proc. Natl. Acad. Sci. U. S. A.*, 2014, **111**, 3624–3630; (*b*) J. Eden, P. R. C. Gascoyne and R. Pethig, *J. Chem. Soc., Faraday Trans.*, 1980, **76**, 426–434.